

A MEMS Fuel Atomizer for Advanced Engines

James Nability*
TDA Research, Inc.
12345 W. 52nd Ave.
Wheat Ridge CO 80033

John Daily†
Center for Combustion and Environmental Research
Department of Mechanical Engineering
University of Colorado at Boulder
Boulder, CO 80309-0427

ABSTRACT

Future aircraft and weapons need highly efficient propulsive power plants to achieve their performance goals. Higher performance engines such as the pulse detonation engine (PDE) are needed. The pulse detonation engine is an exciting airbreathing propulsion cycle with great potential for improved range and thrust. Most research has been performed with gaseous fuels, so demonstrating rapid deflagration-to-detonation using storable, liquid hydrocarbon fuels is essential to successful development and application of this engine. Unfortunately, liquid fuels require atomization unless pre-vaporized, which introduces the challenge of detonating a liquid spray. Recent research shows that droplet Sauter-mean diameters as small as 3 μm may be required for successful detonations. Unfortunately, currently available atomizers produce a droplet distribution that has an unacceptably large number of big droplets (up to 200 μm) even though the Sauter-mean diameter can be as small as 30-40 μm . Thus, new atomization technologies are needed to produce these small droplets. Using microelectromechanical (MEMS) technology, atomizers can be built with the micron scale features needed to obtain very fine droplet atomization. In this paper we describe the design, fabrication and packaging challenges encountered in building a MEMS fuel atomizer for use in advanced engines.

NOMENCLATURE

A area
C capacitance
E modulus of elasticity
f frequency

F force
h, G gap between electrostatically charged plates
I moment of inertia
 k_s diaphragm spring constant
L micropump chamber length
m diaphragm mass
MEMS microelectromechanical systems or structures
p pressure
r radius
SMD Sauter-Mean Diameter
t thickness
u internal energy
v velocity
V voltage
w width
z deflection or displacement

Greek

ϵ_o relative permittivity
 ϵ_r dielectric constant
 μ dynamic viscosity
 ν Poisson's ratio
 θ_c contact angle
 ρ fuel density
 σ surface tension

subscripts

e electrostatic
k spring
l liquid
R residual
s solid

BACKGROUND

The liquid-fueled pulse detonation engine (PDE) is an unsteady device with great potential for improved range

* Member, AIAA and corresponding author,
nability@tda.com or (303) 940-2313.

† Associate Fellow, AIAA

and thrust. However, most research has been performed with gaseous fuels, so demonstrating rapid deflagration-to-detonation using storable, liquid hydrocarbon fuels is essential to the successful development and application of this engine. Unfortunately, liquid fuels require atomization unless pre-vaporized, which introduces the challenge of detonating a liquid droplet spray. Recent research by Brophy, et al. [1-2] shows that droplet Sauter-mean diameters as small as 3 μm may be required. New atomization technologies are needed to produce these small droplets with low supply pressure. The atomizer must also deliver high flow rate, be operable to high temperature, and have high-speed on/off pulsing capability with zero-drip closure. Unfortunately, no single atomization technology can currently perform all functions. Therefore, TDA Research and the University of Colorado-Boulder are developing novel high-speed MEMS atomizer technology.

The high thermodynamic efficiency of the PDE has motivated its development. For example, Wintenberger, et al. [3] shows the expected fuel-based specific impulse of hydrocarbon-air detonations to be about 1600-2000s; significantly greater than the 1100-1200s that can typically be obtained with a liquid-fueled ramjet. Further, the parametric study by Fong and Nalim [4] showed that specific impulse was optimized when the PDE was operated from about 60 to 100 Hz.

Successful PDE operation hinges on the precise occurrence of a timed sequence of events that are sketched in Figure 1. An inlet delivers air to fill the detonation tube. Fuel sprayed into the engine mixes with the air to create a detonable near stoichiometric fuel-air mixture. The PDE generates thrust upon detonation in a confined tube. The detonation wave quickly travels down the length of the tube consuming the reactants. The increased pressure behind the shock wave produces thrust until the hot gases have been exhausted from the detonation tube. After purge the process is then repeated.

Fuel injection into the inlet diffuser is most likely, although injection directly into the main combustor or detonation tube may also be desired. Depending on operating conditions and the engine configuration, the fuel injector face could be exposed to high gas temperature and cyclic detonative pressures exceeding 20 atm. This transient back-pressure makes it necessary to incorporate micro check valves into the fuel feed path to the atomization chamber in order to prevent backflow through the atomizer. At 60Hz cycle speed we expect the fuel injection period per cycle to be 8 msec or less. Therefore, high-speed MEMS fuel

atomizers will be needed to precisely and independently control the fuel injection distribution and cycle time for engine optimization.

In this paper we describe the design, analysis and fabrication of a MEMS atomizer. Fabrication of the necessary atomizer components is fairly straight forward using MEMS micromachining processes. However, the assembly and packaging of silicon chips to create a fuel and temperature compatible atomizer is nontrivial. Also, the dielectric needs to withstand the high voltage applied to the electrodes. This voltage potential generates the electrostatic force that actuates the micropump diaphragm. For these reasons additional development is still needed to achieve reliable operation of an atomizer array.

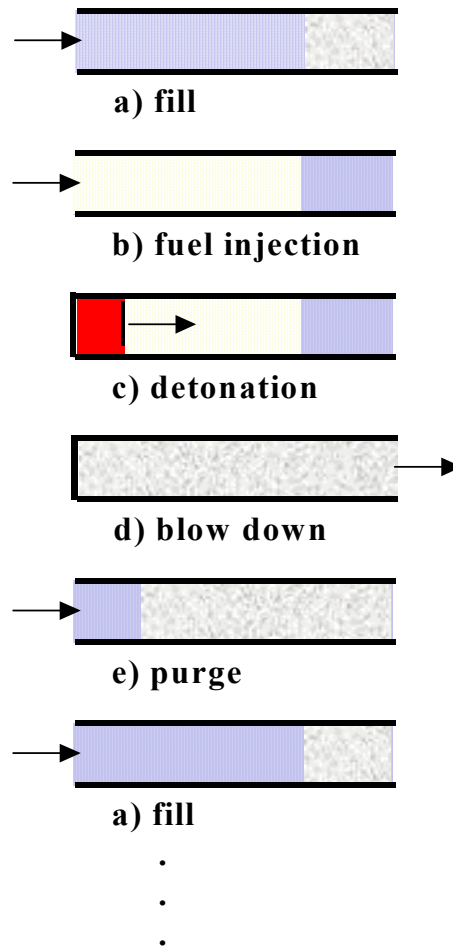


Figure 1. Generic PDE operating sequence.

MEMS ATOMIZER DESIGN

Given the droplet size needed for detonations, the use of inkjet based printer technology comes to mind.

Inkjet printer technology is based on the ability to eject small single droplets on demand at repetition rates high enough for fast printing. This is achieved by building print heads with multiple injectors; each individually addressable and electrically actuated. The injector nozzle size determines the droplet diameter, which is typically $\sim 20\text{-}40\mu\text{m}$ in the printing application. Recent improvements in the technology (driven by the desire for even faster printing and smaller droplets to give better resolution) have resulted in high-speed devices operating at up to 100 kHz and producing drops to less than $20\mu\text{m}$ in diameter.

There are several advantages to this type of fuel injection technology. First, the injector nozzle geometry can be tailored specifically to produce droplets in the desired size range. These microscale flows are typically laminar, and droplet formation is driven by the Rayleigh breakup mechanism. Therefore, droplet size scales approximately with the minor dimension of the injection nozzle. Further, the droplets are always the same size (independent of flow rate), since flow rate is largely controlled by actuation frequency.

For example, TDA measured the droplet distribution of a Seiko- Epson 777 inkjet with a Malvern 2600 particle size analyzer (see Figure 2). The SMD was measured at $40\mu\text{m}$ and the droplet distribution was nearly monodisperse. Only about 10% by volume were larger than $50\mu\text{m}$ in diameter and none were larger than $62\mu\text{m}$. In contrast, Kushari, et al. [5] tested an air-assist atomizer having a greater volume fraction ($\sim 21\%$ for the example shown in the figure) of droplets greater than $50\mu\text{m}$. In fact some droplets were as large as $200\mu\text{m}$.

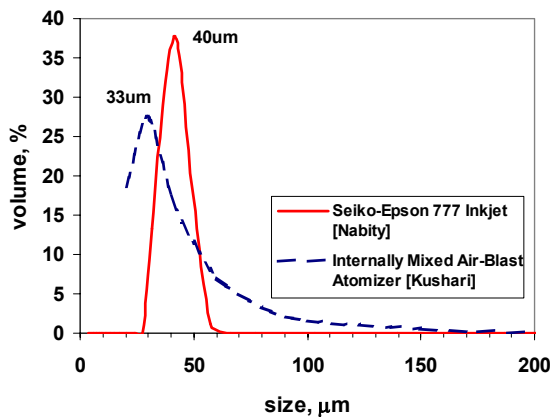


Figure 2. Droplet distributions for inkjet and air-assist atomizers.

The individual nozzles can also be separately addressed (as is the case in printers) using very simple electronics.

That means that one could build an injector array to spatially and temporally control fuel injection to improve detonability. The fuel flow and distribution can be adjusted in real-time to run the engine at peak efficiency for a given power requirement.

Finally, the inkjets are self-aspirating. The diaphragm or pressure plate pumps fluid into the injector and ejects fluid through the nozzle. Therefore, in contrast to conventional atomizers the demand on supply pressure is small.

Our design shown in Figure 3 uses a double-acting diaphragm pump, with an injection cavity on both sides. A manifold delivers fuel through fluidic check valves as electrostatic actuation of the diaphragm pump simultaneously aspirates fuel into one cavity and expels fuel out of the opposing cavity. After exiting the nozzle the expelled fuel breaks up into small droplets.

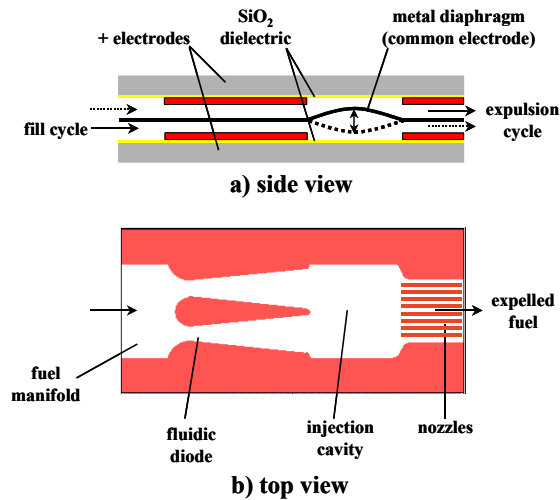


Figure 3. Double acting diaphragm pump configuration and flowpath details.

Electrostatic actuation was selected for our atomizer because it requires much less power than thermal actuation and is less temperature sensitive than piezoelectric actuation. The diaphragm can be electrostatically actuated in either direction by alternating the DC voltage to the electrodes at the desired actuation frequency (Figure 4).

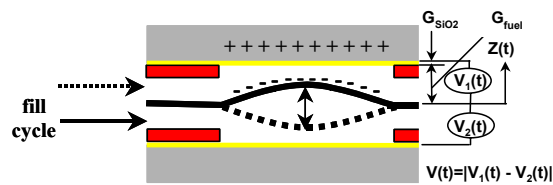


Figure 4. Electrostatic actuation.

An array of atomizer elements can be built up to achieve the desired fuel mass flow with a small surface area. The array also permits controlled distribution of the fuel into the airflow via electronic addressing. The expected spray pattern will have well distributed small droplets ejected normal to the nozzle array surface (much like a shower head; only in this case the length scale for droplet breakup is short due to the small nozzle feature size).

Stiction, voltage breakdown, fouling and packaging make MEMS atomizer development challenging. The design must solve these using materials and processes available to silicon micromachining. For improperly designed MEMS devices, adhesion or stiction commonly causes failure during fabrication or operation. The photo (Figure 5) shows an example of a device that failed during release due to elastocapillary adhesion. This atomizer was fabricated with the MEMSCAP PolyMUMPs™ silicon surface-micromachining process [6], released with buffered hydrofluoric acid to remove the sacrificial oxide layers and then dried using a supercritical CO₂ process. The silicon diaphragm remained free in the center where bumps prevented intimate contact between the two surfaces. However, these bumps were not continued all the way out to the chamber walls and therefore, the outer annulus of the diaphragm collapsed.

In general there are two modes of adhesive failure: 1) capillary condensation (such as occur during MEMS release), and 2) intersolid adhesion. Mastrangelo

analytically and experimentally investigated the adhesion of contacting surfaces [7-10]. He determined that two non-dimensional numbers characterized the tendency of microstructures to adhere to their underlying substrates. The Elastocapillary Number (N_{EC}) is the ratio of the restoring force to the capillary force of attraction, and the Peel Number (N_P) is the ratio of the restoring force to the atomic level intersolid force. In both cases, Mastrangelo defined the numbers so that sticking is avoided for values greater than unity.

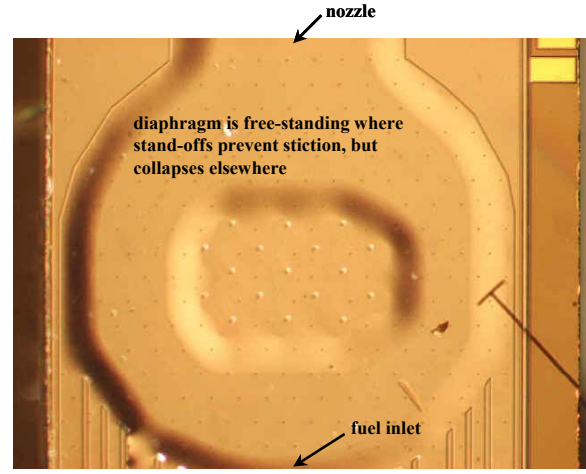


Figure 5. Photo of early TDA PolyMUMPs™ fabricated MEMS atomizer. Failure due to elastocapillary adhesion during release.

Table 1. Adhesion numbers for circular and square plates. [7]

Structure	Elastocapillary Number (N_{EC})
circular plate	$\frac{10}{9} \left(\frac{5}{2} \right)^{\frac{2}{3}} \left(\frac{Eh^2t^3}{\sigma_l \cos \Theta_c (1-v^2)r^4} \right) \left[1 + \frac{3(1-v^2)\sigma_R r^2}{4Et^2} + \frac{2187}{2560} \left(\frac{2}{5} \right)^{\frac{2}{3}} \left(\frac{h}{t} \right)^2 \right]$
square plate	$\left(\frac{25Eh^2t^3}{\sigma_l \cos \Theta_c (1-v^2)w^4} \right) \left[1 + \frac{2(1-v^2)\sigma_R w^2}{9Et^2} + \frac{5}{12} \left(\frac{h}{t} \right)^2 \right]$
	Peel Number (N_P)
circular plate	$\frac{40}{3} \left(\frac{Eh^2t^3}{\sigma_s (1-v^2)r^4} \right) \left[1 + \frac{51(1-v^2)\sigma_R r^2}{160Et^2} + \frac{63}{200} \left(\frac{h}{t} \right)^2 \right]$
square plate	$\left(\frac{186Eh^2t^3}{\sigma_s (1-v^2)w^4} \right) \left[1 + \frac{27(1-v^2)\sigma_R w^2}{310Et^2} + \frac{12}{31} \left(\frac{h}{t} \right)^2 \right]$

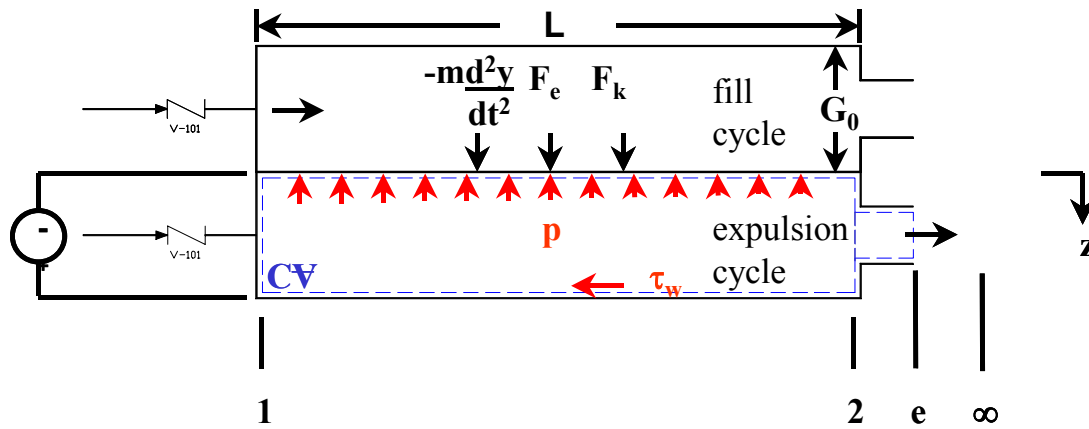
There is always concern that nozzle fouling could arise due to the very small fuel passages. Fouling could be caused by solid contaminant particles in the fuel, fuel tar residues left behind when the fuel evaporates, or by coke formation. First, there are commercially available filter systems that capture all particulates above 0.5 μm . We have used these types of filters successfully in our laboratory testing. Second, fouling due to tar condensation or fuel pyrolysis can be eliminated by pumping the fuel out of the injector during shutdown, thereby avoiding evaporation of stagnant fuel remaining in the flow passages. Third, under conditions expected at the nozzle, the majority of coke will form by one of two mechanisms: a catalytic mechanism that produces carbon filaments or a gas phase mechanism, which is referred to as condensation coke. [11] TDA has developed methods to control each of these coke formation pathways.

A working MEMS atomizer will be tolerant of these as well as other issues. Further, a packaged atomizer must be fuel compatible, seal the atomizer from the environment and have interconnects to access electric power. To address these TDA Research developed simple models to gain insight into electrostatic

actuation, fluid dynamics and droplet breakup. The atomizer analysis model, microfabrication methodology and spray characterization test rig are described below.

MICROPUMP ANALYSIS

A one-dimensional model coupling fluidics, electrostatic actuation and diaphragm structural response was developed to estimate MEMS atomizer pump performance. The problem is one of unsteady flow through a deformable control volume with boundary work acting on the fluid as shown in Figure 6. The sketch depicts the forces and boundary conditions imposed on the model during the fuel expulsion cycle (details of the fill cycle are not shown). The diaphragm is electrostatically actuated towards the positive or bottom electrode; overcoming the diaphragm spring restoring force. Assuming a perfect check valve or fluidic diode, the inlet flow is shut-off once the chamber pressure exceeds the fuel delivery pressure. The volumetric flow rate out of the atomizer is then equal to the volume displaced by the diaphragm, whose movement depends upon the applied electrostatic force.



Continuity:

$$\dot{m}_e = \rho \bar{v}(t) A|_e = \rho \bar{v}(t) A|_i - \rho \frac{dVol}{dt}$$

x momentum:

$$\rho \bar{v}^2(t) A|_i + \rho A|_i + \rho \frac{d}{dt} \left(\iiint_{CV} \bar{v} dV \right) - \frac{12\mu vL}{h} |_f \cdot A_f = \rho \bar{v}^2(t) A|_e + \rho A|_e = \rho \bar{v}^2(t) A|_e + \rho A|_e$$

ΣF of

diaphragm:

$$\Sigma F_z = 0 = \bar{F}_e + \bar{F}_k - \bar{p}A + m\bar{g} + \rho \frac{d}{dt} \left(\iiint_{CV} \frac{d\bar{z}}{dt} dV \right)$$

inertial terms \ll loads and may be neglected

Energy:

$$\int \Delta E dm|_{CV} = \iiint \left(u + \frac{p}{\rho} + \frac{v^2}{2} \right) dm|_{in} - \iiint \left(u + \frac{p}{\rho} + \frac{v^2}{2} \right) dm|_{out} + \int_{z_1}^{z_2} (\bar{F}_e + \bar{F}_k) dz \quad \text{adiabatic, unreacting flow}$$

Figure 6. Unsteady, adiabatic, nonreacting and incompressible flow through a deforming control volume.

The diaphragm pumping process is irreversible, since the flow resistance of a Newtonian fluid between closely spaced parallel plates is substantial. If we assume the flow to be quasi-steady, then we may estimate the viscous flow loss between high-aspect ratio parallel plates to be

$$\Delta P = \frac{12 \cdot \mu \cdot L \cdot v}{h^2} \Big|_{fuel}$$

from Hagen-Poiseuille flow, where the diaphragm and positive electrode represent the plates. For circular or 2-d low-aspect ratio flow channels the Hagen-Poiseuille flow pressure loss is given by

$$\Delta P = \frac{8 \cdot \mu \cdot L \cdot v}{R_h^2} \Big|_{fuel}$$

with R_h the hydraulic radius of the channel. Since our flow is transient, these steady flow relations will only provide a good approximation to the actual pressure loss as long as the total expulsion time is large in comparison to the characteristic time of impulsively started flow.

A summation of forces acting on the diaphragm reveals that the force exerted on the fluid during electrostatic actuation is $\vec{F} = \vec{F}_e + \vec{F}_k$ (self-aspirating pump); $\text{sign}(F_e)$ is always positive, since electrostatics can not generate a repulsive force, and $\text{sign}(F_k)$ will depend on the direction of travel of the diaphragm (+ or - y-direction). Therefore, in self-aspirating mode, F is the motive force to expel fluid through the atomizing nozzles at any time, t .

The electrostatic force is

$$\vec{F}_e(t) = \left[\frac{\frac{1}{2} \varepsilon_o \varepsilon_r \Big|_{fuel} \varepsilon_r^2 \Big|_{dielectric} \cdot V^2(t)}{\left[\varepsilon_r \Big|_{dielectric} (G_{fuel} - \vec{y}(t)) + \varepsilon_r \Big|_{fuel} G_{dielectric} \right]^2} \right] \vec{y}(t)$$

ε_o = relative permittivity = 8.85×10^{-6} pF/um

ε_r = dielectric constant

$V(t)$ = actuation voltage

G = gap (either fuel or dielectric)

$y(t)$ = diaphragm displacement

and the diaphragm spring force is

$$\vec{F}_k(t) = -k_s \cdot \vec{y}(t)$$

k_s = Roark spring constant [12]

The mechanism by which the jet will collapse and breakup into droplets is determined by the properties of the fluid and nozzle geometry. Rayleigh breakup of a laminar jet is expected for flow through small nozzles. Fluid is expelled from a nozzle as a small diameter jet,

which breaks up due to the growth of surface tension induced instabilities as illustrated in Figure 7. The small droplets formed are approximately proportional to twice the nozzle diameter, but smaller satellite droplets can also occur. [13] Accordingly, a 6 μm -diameter nozzle orifice can produce 10 μm droplets.

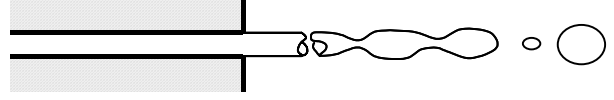


Figure 7. Rayleigh jet breakup.

The model was used to predict the micropump performance with JP-10 fuel. Fluid properties at 21°C are:

$$\rho = 0.94 \text{ gm/cm}^3$$

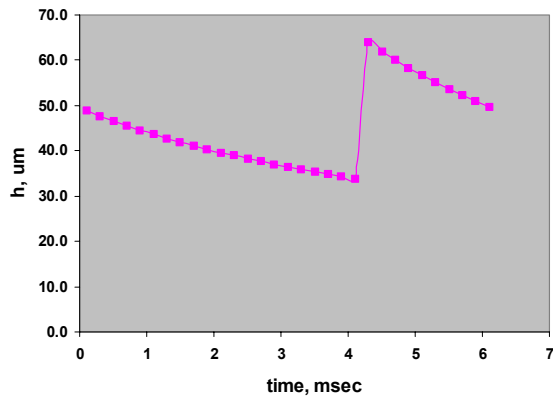
$$\mu = 0.003 \text{ kg/m-s}$$

$$\sigma = 0.031 \text{ N/m}$$

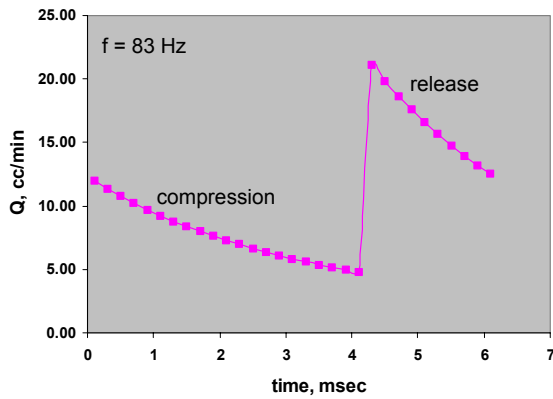
A 50um-thick stainless steel diaphragm was sandwiched by two chips containing a 1 cm x 1 cm x 50 μm pump chamber. The diaphragm was actuated at 83Hz with an applied voltage of 1000VDC. At this frequency the diaphragm was predicted to deflect about 15 μm (Figure 8a) and deliver a time-averaged pump capacity of 11 cm^3/min (Figure 8b). Varying the frequency shows that the optimum pump frequency lies between 50 and 100 Hz (Figure 8c).

FABRICATION

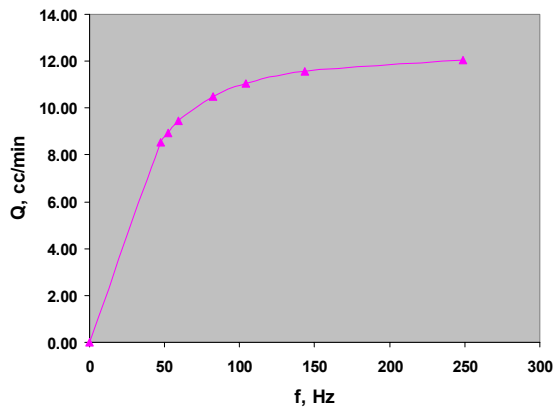
There are several commercial processes for MEMS device fabrication. MUMPs™ [6] and SUMMiT™ [14] are both well-known to the MEMS community for surface micromachining. While these processes are well-suited for prototype development of devices with micron-size features, we cannot use them for larger devices and arrays. Therefore, we bulk micromachine silicon wafers according to a patterned mask using the University of Colorado Electrical Engineering Semiconductor Laboratory. UV lithography transfers the pattern to substrates using a light sensitive photoresist. The photo mask, which can be made by commercial companies in accordance to the required design, is aligned and placed directly on the photoresist-coated substrate, using a Karl Suss MJB3 mask aligner. The transparent regions of the mask permit exposure of the photoresist, which once developed become resistant to the solvent and the unexposed photoresist is washed away. The patterned photoresist layer then patterns the underlying oxide layer in a hydrofluoric acid bath. It is this patterned oxide layer that is used to define 3-dimensional structures in the silicon wafer.



a) chamber height or gap between electrodes



b) flow rate



c) frequency response

Figure 8. Predicted self-aspirating MEMS atomizer pump performance.

The contact force between the mask and photoresist directly correlates with fidelity of the transfer. Figure 9 shows that soft contact degrades the crisp features of the original mask. At the very least we observe rounded corners, and very small features can even be lost.

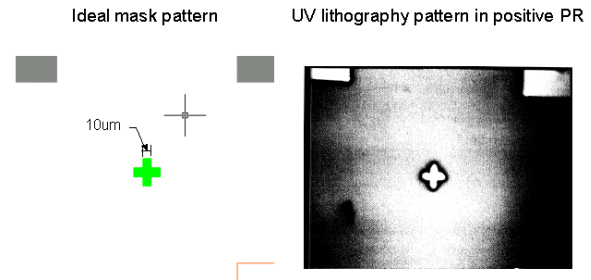


Figure 9. UV lithography soft contact between mask and wafer.

A buffered KOH bath anisotropically etches silicon wafers quickly and with high degree of resolution of features. The KOH etch rates are about 600:1 for the <110> plane and 300:1 for the <100> plane in reference to the <111> plane; thus, features with very large aspect ratios of 100s to 1 can be created. The KOH etchant nearly stops upon contact with the thermal oxide dielectric layer leaving the patterned features. Thus, well-defined fuel passages can easily be etched to 10's of microns deep as shown in Figure 10. Electric wire bond pads can be vapor deposited if desired.

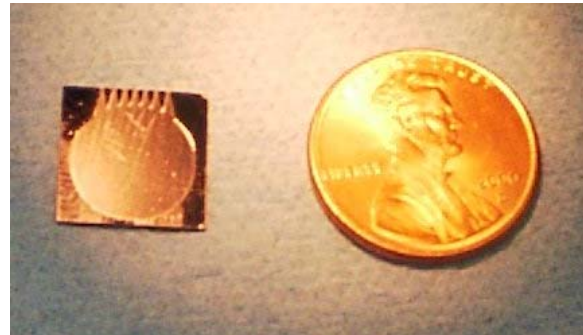


Figure 10. TDA Research/ UC-Boulder surface micromachined atomizer chip; smaller than a penny.

After wafer dicing, we bond a metal foil diaphragm between two etched chips to form a single MEMS atomizing element. Electrical leads and a hose connection are attached prior to encapsulating the entire assembly in fuel compatible epoxy. A finished MEMS atomizer assembly is shown in Figure 11. Additional design will be needed to efficiently package an array of atomizer elements.

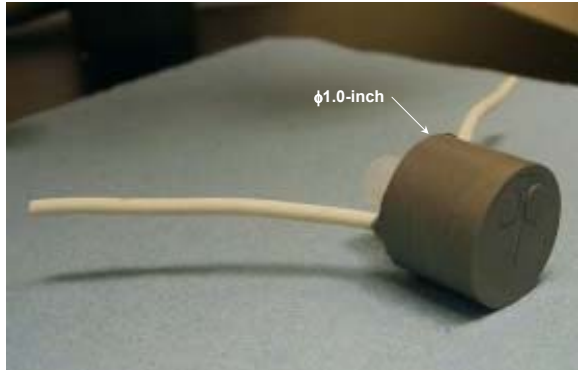


Figure 11. Assembled and packaged MEMS fuel atomizer.

SPRAY CHARACTERIZATION TESTS

Positive pressurization of a piston accumulator fuel tank supplies JP-10 fuel to the atomizer. A two-stage filtering process is used to remove particulates down to $0.5 \mu\text{m}$. The fuel is metered through a fuel control valve prior to delivery to the atomizers. A flow meter for less than $10 \text{ cm}^3/\text{min}$ flow range could not be found, so we calibrate the atomizer nozzle for various supply pressures and actuation voltages by measuring the expelled fuel mass over a known time interval. The calibration curves were used to estimate fuel flow. Fuel control is achieved through pulse-width modulation of the atomizer and through open loop command of a primary fuel control valve.

Droplet distribution data is obtained using a Malvern Mastersizer Particle Analyzer. Nitrogen flow purges the atomizer fixture shown in Figure 12, and then the fuel-nitrogen mixture is exhausted through a liquid trap by the facility vacuum system.



Figure 12. Malvern Mastersizer with nitrogen purged fuel injection fixture.

Microscope imaging systems are used to obtain close-up photos of the ejection and breakup process. As an example, Figure 13 shows a photo taken of an HP 51645A inkjet thermally actuated at 300 Hz. The primary droplet size was estimated at $30 \mu\text{m}$ and the satellite droplets to be about $15\text{-}20 \mu\text{m}$ by comparing the droplet diameters to the solder balls visible at the left. There were about 4 satellite droplets per ejection, so the SMD was determined to be about $23 \mu\text{m}$. A droplet diameter of $35 \mu\text{m}$ was calculated based on the measured mass of the droplets (reasonably good agreement with the measurements off of the image).

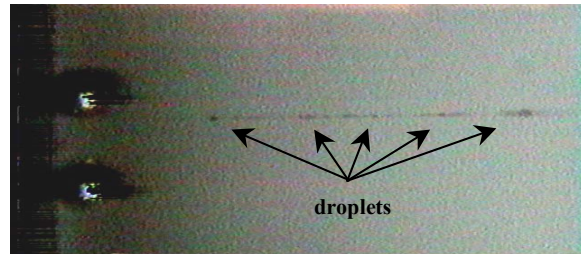


Figure 13. HP 51645A fired at 300Hz.

CONCLUSIONS

A MEMS fuel atomizer has been designed for the PDE, and is also applicable to other advanced engines. Nearly monodisperse droplets smaller than $10 \mu\text{m}$ should be produced. Performance predictions made with analytically based models show that the atomizer will flow about $11 \text{ cm}^3/\text{min}$ in self-aspirating mode.

Microfabrication processes were used to create atomizing chips that were then assembled and packaged for initial testing. Pressurized flow tests showed that fuel flows well through the micro passages without fouling. Atomizer actuation and fuel expulsion tests will be conducted shortly; we will measure the droplet size distributions using particle analyzer and flow visualization setups.

ACKNOWLEDGEMENT

An ONR Phase II SBIR supported this work under contract number N00014-01-C-0457. Dr. Chris Brophy, Naval Postgraduate School, Monterey, CA was technical monitor.

REFERENCES

1. C.M. Brophy, D.W. Netzer, J. Sinibaldi, and R. Johnson, "Detonation of a JP-10/Aerosol for Pulse Detonation Applications," ONR PDE Workshop, Russia, July 2000.

2. C.M. Brophy, J.O. Sinibaldi, D.W. Netzer, and R.G. Johnson, "Operation of a JP-10/Air Pulse Detonation Engine," 36th AIAA/ASME/SAE/ASEE Joint Propulsion Conference, 17-19 July 2000, Huntsville, Alabama. AIAA Paper 2000-3591.
3. E. Wintenberger, J. M. Austin, M. Cooper, S. Jackson, and J. E. Shepherd, "Analytical Model for the Impulse of Single-Cycle Pulse Detonation Tube," *Journal of Propulsion and Power*, Vol. 19, No. 1, pp. 22-38 January-February 2003.
4. K.K. Fong and M. Razi Nalim, "Gas Dynamic Limits and Optimization of Pulsed Detonation Static Thrust," 36th AIAA/ASME/SAE/ASEE Joint Propulsion Conference, 17-19 July 2000, Huntsville, Alabama. AIAA Paper 2000-3471.
5. A. Kushari, Y. Neumeier, O. Israeli, E. Lubarsky, and B.T. Zinn, "Internally Mixed Liquid Injector for Active Control of Atomization Process," *Journal of Propulsion and Power*, Vol. 17, No. 4, July-August 2001.
6. David A. Koester, Allen Cowen, Ramaswamy Mahadevan, and Busbee Hardy, *PolyMUMPS™ Design Handbook Revision 8.0*, MEMSCAP Inc, 2002. <http://www.memsrus.com/mumps.pdf> [cited 9 August 2004].
7. C.H. Mastrangelo, "Adhesion-Related Failure Mechanisms in Micromechanical Devices," *Tribology Letters*.
8. C.H. Mastrangelo and C.H. Hsu, "Mechanical Stability and Adhesion of Microstructures Under Capillary Forces---Part I: Basic Theory," *Journal of Microelectromechanical Systems*, Vol. 2, No. 1, March 1993, pp. 33-43.
9. C.H. Mastrangelo and C.H. Hsu, "Mechanical Stability and Adhesion of Microstructures Under Capillary Forces---Part II: Experiments," *Journal of Microelectromechanical Systems*, Vol. 2, No. 1, March 1993, pp. 44-55.
10. C.H. Mastrangelo and C.H. Hsu, "A Simple Experimental Technique for the Measurement of the Work of Adhesion of Microstructures," IEEE paper 0-7803-0456-X/92, 1992.
11. Baker, R. T. K., Yates, D. J. C., and Dumesic, J. A. (1982). "Filamentous Carbon Formation Over Iron Surfaces," in *Coke Formation on Metal Surfaces*, ACS Symposium Series 202, 1.
12. Warren Young and Richard Budynas, *Roark's Formulas for Stress and Strain*, 7th edition, published by McGraw-Hill, 2001.
13. Lefebvre, A., 1989, *Atomization and Sprays*, published by Hemisphere Publishing Company.
14. SUMMiT™
<http://www.sandia.gov/mstc/technologies/micromachines/tech-info/technologies/trilevel.html> [cited 9 August 2004].